

The host galaxies of luminous radio-quiet quasars

W.J.Percival,^{1,2} L.Miller,¹ R.J. McLure^{2,1} and J.S. Dunlop²

¹ Dept. of Physics, University of Oxford, Nuclear & Astrophysics Laboratory, Keble Road, Oxford OX1 3RH, U.K.

² Institute for Astronomy, University of Edinburgh, Royal Observatory, Blackford Hill, Edinburgh EH9 3HJ, U.K.

Submitted for publication in MNRAS

ABSTRACT

We present the results of a deep K -band imaging study which reveals the host galaxies around a sample of luminous radio-quiet quasars. The K -band images, obtained at UKIRT, are of sufficient quality to allow accurate modelling of the underlying host galaxy. Initially, the basic structure of the hosts is revealed using a modified Clean deconvolution routine optimised for this analysis. 2 of the 14 quasars are shown to have host galaxies with violently disturbed morphologies which cannot be modelled by smooth elliptical profiles. For the remainder of our sample, 2D models of the host and nuclear component are fitted to the images using the χ^2 statistic to determine goodness of fit. Host galaxies are detected around all of the quasars. The reliability of the modelling is extensively tested, and we find the host luminosity to be well constrained for 9 quasars. The derived average K -band absolute K -corrected host galaxy magnitude for these luminous radio-quiet quasars is $\langle M_K \rangle = -25.15 \pm 0.04$, slightly more luminous than an L^* galaxy. The spread of derived host galaxy luminosities is small, although the spread of nuclear-to-host ratios is not. These host luminosities are shown to be comparable to those derived from samples of quasars of lower total luminosity and we conclude that there is no correlation between host and nuclear luminosity for these quasars. Nuclear-to-host ratios break the lower limit previously suggested from studies of lower nuclear luminosity quasars and Seyfert galaxies. Morphologies are less certain but, on the scales probed by these images, some hosts appear to be dominated by spheroids but others appear to have disk-dominated profiles.

Key words: galaxies: active, quasars: general, infrared: galaxies

1 INTRODUCTION

Models of the cosmological evolution of quasars often use galaxy mergers as the primary mechanism for quasar activation and require the mass of the structure within which a quasar is formed as a basic parameter (Efstathiou & Rees 1988; Haehnelt & Rees 1993; Percival & Miller 1999). One step towards testing hypotheses about quasar initiation is to answer the question: Is a quasar's luminosity correlated with the luminosity of the structure within which it formed? Such a correlation has been shown to exist for low redshift ($0 < z < 0.3$) Seyferts and quasars with luminosities $M_V \gtrsim -25$ in that there appears to be a lower limit to the host luminosity which increases with quasar luminosity (McLeod & Rieke 1995; McLeod, Rieke & Storrie-Lombardi 1999). However this limit is poorly defined, particularly for high luminosity quasars when the strong nuclear component makes it increasingly more difficult to find low luminosity hosts.

Recent work has shown that the majority of nearby galaxies have massive dark objects in their cores, which are

suggested to be super-massive black holes potentially capable of powering AGN (Kormendy & Richstone 1995; Magorrian *et al.* 1998). These studies have also found evidence for a correlation between the mass of the compact object and the luminosity of the spheroidal component of the host. Assuming a link between nuclear luminosity and black hole mass, the average nuclear luminosity emitted by low redshift quasars is expected to increase with host spheroidal luminosity. In light of this prediction there has been a resurgence of interest in host galaxy studies and recent work (McLure *et al.* 1999) has found weak evidence for a correlation in accord with the relations of Magorrian *et al.* (1998). However, this correlation relies on spheroid/disk decomposition for two quasars with low nuclear luminosities, and only a small number of luminous radio-quiet quasars were observed.

Host galaxy properties of AGN are known to be correlated with the radio power: radio galaxies tend to be large spheroidal galaxies, while disk galaxies tend to be radio-quiet. Recent evidence suggests that the hosts of radio-loud quasars are also predominantly massive spheroidal galaxies regardless of the nuclear luminosity (Dunlop *et al.* 1993;

Taylor *et al.* 1996; McLure *et al.* 1999). However, studies of radio-quiet quasars with luminosities $M_V \gtrsim -25$ have shown that the hosts can be dominated by either disk-like or spheroidal components or can be complex systems of gravitationally interacting components (Taylor *et al.* 1996; Bahcall *et al.* 1997; Boyce *et al.* 1998; McLure *et al.* 1999). There is therefore strong justification for studies to see if these luminosity and morphological trends extend to the hosts of more luminous ($M_V \lesssim -25$) radio-quiet quasars.

There have been many recent detections of host galaxies in the optical thanks to results from HST (Hooper, Impey & Foltz 1997; Bahcall *et al.* 1997; Boyce *et al.* 1998; McLure *et al.* 1999), which add to our knowledge from ground-based studies (Malkan *et al.* 1984a; Malkan 1984b; Hutchings & Neff 1992; Veron-Cetty & Woltjer 1990). However, quasar hosts often appear significantly disturbed, as if by interaction or merger which can lead to strong bursts of star-formation and significant extended line and blue continuum emission at optical wavelengths which are not indicative of the mass of the underlying host. The nuclear-to-host light ratio in the optical is also typically higher than at longer wavebands.

These problems can be circumvented by observing in the infrared where the contrast between host and nuclear component is improved and the emission associated with star bursting activity is largely absent: the K magnitude is a better measurement of the long-lived stellar populations in the host (Bruzual & Charlot 1993). Previous observations in the infra-red have been successfully used to determine quasar host galaxy luminosities and morphologies (McLeod & Rieke 1994a,b; Dunlop *et al.* 1993; Taylor *et al.* 1996). However, recent advances in telescope design, in particular the advent of adaptive optics systems such as the tip-tilt system on UKIRT produce clearer images of quasars and enable accurate point spread functions (psfs) to be more readily obtained as differences between successive observations are reduced. Such advances coupled with improved analysis techniques mean we are now able to reveal the host galaxies of luminous quasars with $M_V \lesssim -25$ using infra-red observations.

In order to obtain enough luminous radio-quiet quasars our sample was forced to cover redshifts $0.26 \leq z \leq 0.46$. At such redshifts, with typical seeing, the structure of the host galaxy is hidden in the wings of the psf from the nuclear component. There are two main ways of proceeding: either the psf can be deconvolved from the quasar light to directly observe the host galaxy, or known galaxy profiles can be used to model the hosts, a nuclear component can be added in and the profiles can be fitted to the data. Because the host galaxies sometimes have disturbed morphologies indicative of violent mergers, it is difficult to assume a form for the galaxy. However without such modelling, it is not easy to determine the contribution of the host to the light from the centre of the quasar and deconvolution routines tend to produce biased solutions which may alter important features.

For the analysis of our quasar sample, an approach is adopted which uses both methods. Initially (Section 5) the images were restored using a deconvolution algorithm, based on the Clean algorithm (Högbom 1974), developed for this problem, which will be described elsewhere (Percival & Miller 2000). This routine was used to reveal the

extent to which the ‘nebulosity’ around the point source is disturbed. Deconvolution of the light from two of our quasars reveals violently disturbed host galaxies indicative of close merger events. In the remainder of our sample, the non-nuclear light is more uniformly distributed around the centre of the quasar. We should note that the resolution provided by this deconvolution technique is probably not sufficient to reveal evidence for weak mergers, where the host galaxy is only slightly disturbed.

Where the image-restoration routine revealed approximate elliptical symmetry in the non-nuclear component, 2D galaxy profiles were fitted to the hosts. Analysis of non-interacting, low redshift galaxies has shown that an empirical fit to both disk and spheroidal systems is given by:

$$\mu = \mu_o \exp \left[- \left(\frac{r}{r_o} \right)^{1/\beta} \right]. \quad (1)$$

where μ is the average surface brightness in concentric elliptical annuli around the core, and r is the geometric average of the semi-major and semi-minor axes.

Model images were carefully created using this profile and were tested against the data using the χ^2 statistic to determine goodness of fit. Five host parameters were required, the half-light radius, integrated luminosity, axial ratio, angle on the sky, and the power-law parameter of the galaxy β , as well as the nuclear-to-host ratio. Section 6 describes the modelling procedure in detail, and in Section 8 the best-fit parameters are presented for the host galaxies.

Much previous work has produced ambiguous results because of a lack of error analysis and insufficient testing of the modelling. A detailed analysis of the reliability of the 2D modelling method used in this paper has therefore been undertaken and is presented in Section 7. Although hosts are detected in all of our sample, the upper limit of the host luminosity is only usefully constrained for 9 of the 12 quasars modelled (see Section 8.1). Similar analysis of the best-fit β parameter which determines the morphology of the host reveals that this parameter is, unsurprisingly, more poorly constrained than the luminosity. However, we have created Monte-Carlo simulations of images with the same signal-to-noise as the original images (Sections 9 & 10). By analysing these images using exactly the same procedure as for the original data we find that it is possible to distinguish between disk and spheroidal structure.

Unless stated otherwise we have adopted a flat, $\Lambda = 0$ cosmological model with $H_0 = 50 \text{ km s}^{-1} \text{ Mpc}^{-1}$ and have converted previously published data to this cosmology for ease of comparison.

2 THE SAMPLE AND OBSERVATIONS

We have selected 13 luminous ($M_V \leq -25.0$) quasars and one less luminous quasar within the redshift range $0.26 \leq z \leq 0.46$. The quasars were checked for radio loudness using the NVSS survey (Condon *et al.* 1998). Three of the 14 quasars were detected at 1.4 GHz in this survey (see Table 1) but their flux densities are all $< 10^{24} \text{ W Hz}^{-1} \text{ Sr}^{-1}$ and they are considered part of the radio-quiet population. Three quasars, 0137-010, 0316-346 and 2233+134 were observed at UKIRT before the tip-tilt system was operational

quasar	J2000 coords		V	z	M_V	1.4 GHz Flux density /W Hz $^{-1}$ sr $^{-1}$	Observing run	Integration time /s
0043+039	00 45 47.3	+04 10 22.5	16.0	0.384	-26.0	-	09/1997	2800
0137-010	01 40 17.0	-00 50 03.0	16.4	0.335	-25.3	1.46×10^{23}	09/1996	11300
0244-012	02 46 51.8	-00 59 32.3	16.5	0.467	-25.9	-	09/1997	10300
0316-346	03 18 06.5	-34 26 37.1	15.1	0.265	-26.0	-	09/1996	6400
0956-073	09 59 16.7	-07 35 18.9	16.5	0.327	-25.1	-	05/1998	8000
1214+180	12 16 49.1	+17 48 04.1	16.7	0.374	-25.2	-	05/1998	7590
1216+069	12 19 20.9	+06 38 38.4	15.7	0.334	-26.0	-	05/1998	7200
1354+213	13 56 32.9	+21 03 51.2	15.9	0.300	-25.5	-	05/1998	8600
1543+489	15 45 30.2	+48 46 08.9	16.1	0.400	-26.0	-	05/1998	14300
1636+384	16 38 17.6	+38 22 49.0	17.0	0.360	-24.8	-	05/1998	7100
1700+518	17 01 24.9	+51 49 20.4	15.1	0.290	-26.2	7.18×10^{23}	09/1997	3600
2112+059	21 14 52.6	+06 07 42.5	15.5	0.466	-26.7	2.95×10^{23}	09/1997	15100
2233+134	22 36 07.7	+13 43 55.0	16.7	0.325	-26.9	-	09/1996	6400
2245+004	22 47 41.6	+00 54 57.3	18.5	0.364	-23.4	-	09/1997	11100

Table 1. The sample of 14 quasars observed. M_V was calculated for each quasar from apparent magnitudes given in the catalogue of Hewitt & Burbidge (1993) assuming no K -correction. Radio fluxes were determined using the NVSS 1.4 GHz survey. Only 3 of the quasars were detected in this survey and their radio fluxes are below the radio-quiet/loud cutoff. We observed this sample in 3 observing runs at UKIRT. For the 09/1996 run, the tip-tilt system was not operational and the psf stars are not expected to be as well matched to the quasars as for the other runs (see Section 3). Note that coordinates given were determined using the original finding charts and the Digitised Sky Survey and may be different from those in the catalogue of Hewitt & Burbidge (1993) which are often inaccurate.

and so these data are not of the same quality as those from subsequent runs.

Of the 13 luminous quasars selected, three, 0956-073, 1214+186 and 1636+384 have not had previous attempts to measure host magnitudes and morphologies. It is difficult to assess the significance of claimed host detections for the other quasars and the associated parameters calculated because of the lack of error analysis which abounds in this field, and the great potential for systematic errors caused by the requirement for accurate psf measurements. However, individual results from these studies are compared to the results of this paper in Section 8.4.

The observations were all taken using the 256×256 pixel InSb array camera IRCAM 3 on the 3.9 m UK Infrared Telescope (UKIRT). The pixel scale is 0.281 arcsec pixel $^{-1}$ which gives a field of view of ~ 72 arcsec. Our sample of quasars was observed during three observing runs in 09/1996, 09/1997 and 05/1998. For the later two runs the image quality was exceptional with consistent FWHM of 0.45 arcsec observed.

The K -band quasar images were taken using a quadrant jitter pattern. This cycled 2 or 4 times through a 4-point mosaic placing the quasar in each of the quadrants in turn. The actual position of the central value within each quadrant was shifted slightly for each image to reduce the effect of bad pixels. Each image consists of ~ 100 secs of integration time divided into exposures calculated to avoid saturation. The exposures varied between 5-10 secs for the quasars alone, down to 0.2 secs for the quasars with a bright star on the chip which we hoped to use as a psf star. Standard stars from the sample of UKIRT faint standards (Casali & Hawarden 1992) were observed for photometric calibration between observations of different quasars. All of the images were corrected for the non-linear response of IRCAM 3 using a formula supplied by the telescope support staff.

3 OBTAINING THE CORRECT PSF

Obtaining an accurate psf is vital to the analysis of the images. With these ground-based observations the psf varies with seeing conditions and telescope pointing. An experimental psf was therefore determined for each of the quasars by observing a nearby bright star. This led to an unbiased, accurate psf without recourse to the quasar images. For three of the quasars, 0956-073, 1214+180 and 1216+069 there was a nearby star which could be placed on the frame with the quasar. This gave an accurate psf measurement with no loss of integration time on the quasar. If required, the position of the quasar for each observation was altered slightly to allow both the quasar and psf to be well within the boundaries of the chip. For the remaining quasars the telescope was offset to a nearby bright star to use as the psf, before and after each quasar integration (which lasted a maximum of 1600 secs). A number of psf measurements were therefore obtained for each night and each quasar. To ensure consistent adaptive optics correction, properties of the tip-tilt guiding were matched between quasar and psf measurements. To do this psf stars were selected to enable tip-tilt guiding from a star of a similar magnitude, distance from the object, and position angle to that used for the quasar image. Magnitudes of the stars chosen to provide a psf measurement are given in Table 3. By examining fine resolution contour plots of the psf images, it was found that the psf was stable over the course of each night, but varied between nights at the telescope and for different telescope pointing. Because of this, the final stacking of psf images was performed with the same weighting between days as for the quasar images (see Section 4).

As a test of the effectiveness of this procedure to provide the correct psf, the fit between measured psf and image for quasar 1543+489 has been compared to the fit between psfs measured for different quasars and the same image. Fig. 1 shows the radial profile of $\sigma^2(\text{image} - \text{psf})$ calculated in circular annuli of width 0.5 arcsec. Here the psf has been scaled

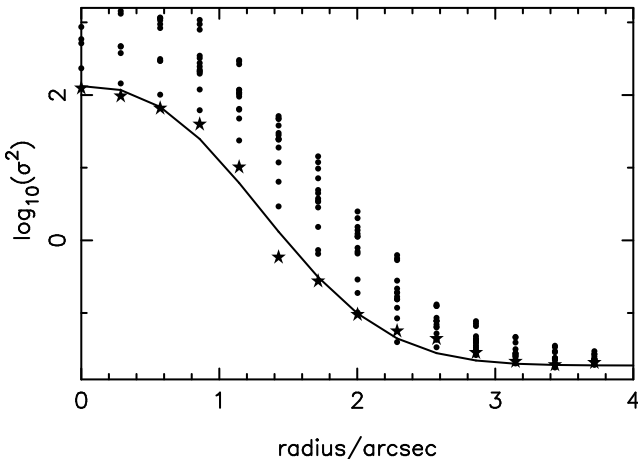


Figure 1. The radial profile of the variance (measured in annuli of width 0.5 arcsec) of the difference between the image of quasar 1543+489 and the scaled psf obtained using the procedure in Section 3 (stars). For comparison, the profiles of the variance obtained using the 13 other psf measurements are also plotted (solid circles). The solid line is the best fit model to the variance, calculated as in Section 6.3.

so the total intensity is the same for both quasar and psf. As can be seen, the psf observed with the quasar image matches the quasar close to its centre better than any other psf. As the core of the psf is undersampled and the sampling between psf and image has not been matched (see Section 6.2 for further discussion of this), this result demonstrates the validity of the psf measuring technique.

4 THE DATA REDUCTION

The data reduction procedure was optimised to search for low surface brightness extended objects. The same procedure was used for both image and psf data so no extra differences between measured and actual psf were introduced. In calculating the flat-field for each mosaic, it was decided to ignore all pixels within the quadrant containing the quasar. This ensured that the flat-fielding technique was not biased to remove or curtail extended emission which could occur if a routine based on pixel values, such as a σ -clipping routine, was used. Outside this quadrant, any areas occupied by bright stars were also removed from the calculation. The sky background level, assumed to be spatially constant was also calculated ignoring these areas.

As the images were undersampled in the central regions we decided to use a sub-pixel shifting routine to centralise the images before they were median stacked to provide the final composite. Having replaced bad pixel values, the images were shifted using a bicubic spline interpolation routine in order to equalise the intensity weighted centres, and were median stacked. Because the psf quality was found to vary from day-to-day, the final stacking of psf images was performed with the same weighting between days as for the quasar images.

Finally, any nearby bright objects in the psf frame were replaced by the average in an annulus of width 0.5 arcsec at the distance of the object from the centre of the psf, around the centre. In the quasar frame any nearby objects were

noted and blanked out of the error frame so they were not included when measuring χ^2 between image and model (see Section 6).

5 DETERMINING SIMPLE MORPHOLOGY

Because of the often disturbed morphology of quasar hosts it is not possible to immediately assume a form for the galaxy structure. For instance if the host is involved in a close merger, modelling it with a smooth profile will not provide the correct host luminosity. The extended wings of the psf from the intense nuclear component hide the host galaxy sufficiently that direct observation cannot easily reveal even violently disturbed morphologies. Simply subtracting a multiple of the psf from the centre of the image will reveal some structure, but a deconvolution routine will reveal more structure. The routine used was a modified Clean algorithm developed for this problem which will be described elsewhere (Percival & Miller 2000). The results show that this routine was of sufficient quality to reveal the approximate symmetry of the host on a scale which includes most of the light important for modelling the galaxy.

Examination of the deconvolved images revealed a clear distinction between disturbed and symmetric systems. Two of the quasars have morphologies which showed no sign of elliptical symmetry and instead show signs of recent merger. The deconvolved images of these quasars are shown in Fig. 2. From these images a value for the non-nuclear luminosity was obtained by summing the residual light excluding the central pixel. Unfortunately the non-nuclear structure revealed was not of sufficient quality to be extrapolated into the central region so the amount of nuclear light which originates in the host galaxy is unknown. Magnitudes obtained from these deconvolved images should therefore be treated as approximate. The structure revealed for these quasars is discussed in Section 8.4. Deconvolving the remaining quasars revealed host galaxies with approximate elliptical symmetry.

6 MODELLING THE QUASAR IMAGES

Having determined that the extended structure around a quasar did not show signs of a disturbed morphology indicative of a close merger and revealed approximate elliptical symmetry, the luminosity and morphology of the host galaxy were estimated by fitting model images to the data. A χ^2 minimisation technique described below was used to estimate the goodness of fit of the models.

6.1 Producing a model galaxy

In this Section we describe how the empirical galaxy surface brightness profile given by Equation 1 was used to estimate the contribution from the host to the counts in each pixel. This had to be done carefully because of the poor sampling of the images. The profile given by Equation 1 has proved to be an excellent fit to many different types of galaxy (Caon, Capaccioli & D'Onofrio 1993; Baggett, Baggett & Anderson 1998) and it is assumed that, if the hosts are not undergoing violent merger, this profile provides a good representation of the galaxy light.

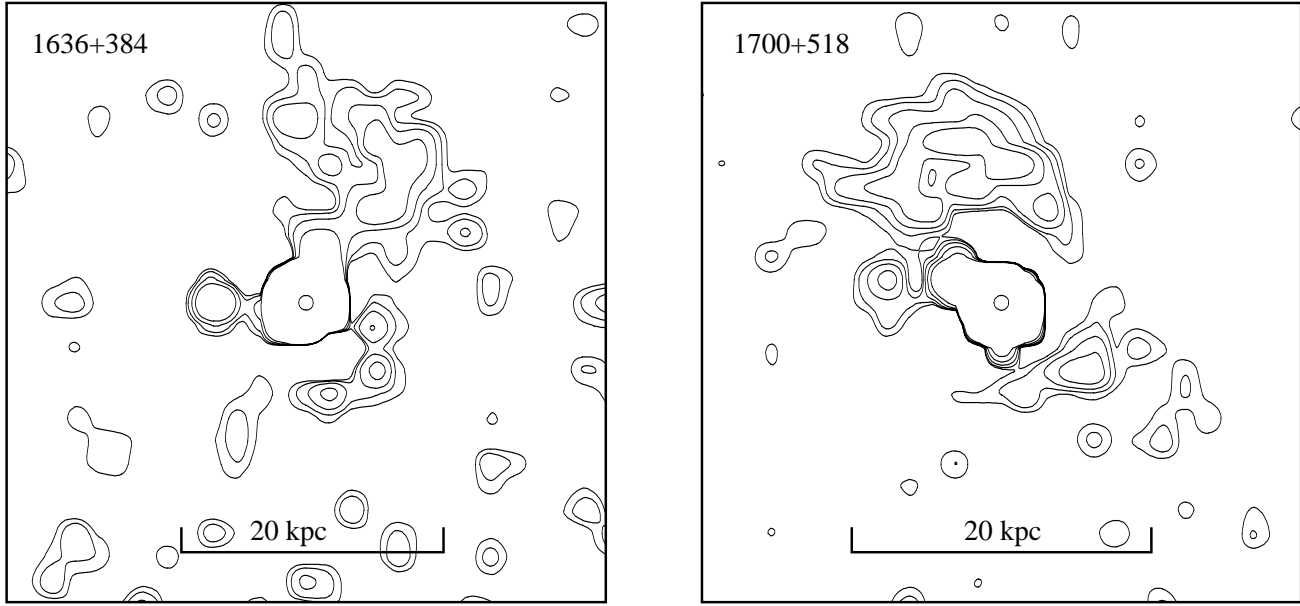


Figure 2. The results of the deconvolution of quasars 1636+384 and 1700+518 revealing hosts with disturbed morphologies indicative of close merger events. The deconvolution output, obtained on the pixel scale, has been smoothed by convolving with a Gaussian with $\sigma = 0.5$ pixels and the residual frame remaining after the algorithm has finished had been added back in to preserve luminosity. Contours are shown at 0.0125%, 0.025%, 0.05% and 50% of the peak intensity. For quasar 1700+581 a contour is also included at 0.00625% of the peak intensity. The size of the images is 7.3×7.3 arcsec (26×26 pixels). See Section 8.4 for further discussion of the morphologies revealed.

Before the method is described, it is useful to revise how an image is obtained from the light emitted by the quasar. Initially, the continuous distribution of light is altered by the atmosphere and the optics of the telescope in a way approximately equivalent to convolution with a continuous point spread function. The resulting continuous distribution is sampled by the detector which integrates the light over each pixel. This is equivalent to convolving the light with a square function of value 1 within a pixel and 0 otherwise, and sampling the resulting distribution assuming uniform response across each pixel. The dithering and subsequent stacking of the images will provide another convolution, although by sub-pixel shifting the images prior to stacking, the effective smoothing width of this function is reduced to less than 1 pixel. The whole process can therefore be thought of as convolving the true psf, the quasar light and a narrow smoothing function (of width ~ 1 pixel) and sampling the resulting continuous image on the pixel scale.

Because the psf measurements were obtained using exactly the same procedure as the quasar images, the measured psf is the result of a convolution of the true psf with the narrow smoothing function. Convolution is commutative and associative so this smoothing function is accounted for in the measured psf and further smoothing of the model galaxy is not required. For this reason the unconvolved model galaxy should not be obtained by simply integrating the model profile over each pixel. Sampling the model galaxy profile onto a grid with spacing equivalent to the pixel scale and convolving with the psf will not produce a correct model galaxy because of aliasing.

In order to limit the aliased signal, the procedure adopted was to extrapolate the psf onto a grid which was finer than the pixel scale using a sinc function (so no ex-

tra high frequency components are introduced). The surface brightness of the model galaxy was then calculated at each point on a grid of the same size and was convolved with the psf on this grid. To provide the final model, this distribution was subsampled onto the pixel scale. Progressively finer grids were used until the total counts in the sampled model galaxy converged, when the majority of the aliased signal is assumed to have been removed. The algorithm adopted used a fine grid with $4 \times$ the number of points at each successive step, and was stopped when the average of all the counts differs from that of the previous step by a factor less than 0.01.

Unless stated otherwise, all model host luminosities and magnitudes which relate to a 2D profile should be assumed to have been integrated to infinite radius. For the large radius within which such models were fitted to the data, this makes only a small difference in the luminosity. The four parameters of the host galaxy are the geometric radius of the elliptical annulus which contains half of the integrated light $R_{1/2}$, the total integrated host luminosity L_{int} , the projected angle on the sky α , the axial ratio a/b and the power law parameter β . In this paper, the integrated host luminosity is quoted in counts /analogue data units (adu) detected in a 1 sec exposure.

6.2 The nuclear component

In principle, adding in the nuclear light is simple - the correct amount is added to the centre of the model galaxy to minimise χ^2 between model and observed images. However, it is important to account for all of the nuclear light. Differences between measured and true psf caused by undersampling, seeing variations or effects such as telescope shake must be

accounted for, even though the adopted observing strategy has limited some of these. In particular, when a nearby star (as used in Section 7.5) is deconvolved, the resulting light appears not only in the central pixel, but in the surrounding pixels as well: if similar components from the nuclear light are not accounted for in the quasar images, the host luminosities and morphologies derived will be wrong.

Because of the large peak in both the image and psf, trying to alter the sampling of the images by extrapolating onto a fine grid and resampling without inducing unwarranted frequency components causes ‘ringing’ in the images which is large enough to affect the results of the modelling. It would be possible to use a different extrapolation technique, but this risks altering the image and measured psf in different ways. Instead, a more simple correction to this problem is adopted: rather than only adding a multiple of the psf to the central pixel, variable multiples of the psf are also added centred on the surrounding 8 pixels. In the perfect case where the measured psf is accurate, while such free parameters make convergence to the minimum χ^2 value slower, they do not affect the position of the minimum: the additional components make a negligible contribution to the model. However, suppose there is a discrepancy between measured and true psf so that the deconvolved image of the nuclear light consists of a central spike surrounded by corrective components which decrease in magnitude with distance away from the spike. Allowing the value of the pixels close to the core to be free parameters in our model will correct these discrepancies and any light observed originating away from the core will be more likely to be from the host galaxy and not from escaping nuclear light. The opposite is also true, and these extra components will also correct psf measurement errors which cause light from the galaxy to be wrongly ascribed to the core (as for quasar 0956–073: see below). Undersampling problems do not affect the modelled galaxy to the same extent because the galaxy light is more uniformly distributed and discrepancies are smoothed. In particular, the total integrated light measured to be from the host will only be minimally affected: see below.

Quasar 0956–073 was modelled using different numbers of these extra components, and the recovered host parameters are given in Table 2. As expected, the χ^2 value decreases with an increasing number of additive psf components showing that the fit between model and image is being improved. The recovered parameters for 1 or 9 additive components show moderate differences, but allowing more components makes no further significant change. Because the host luminosity increases for this quasar with increasing numbers of added components, the sum of the extra psf contributions must be negative which suggests that, for this quasar, the psf has a slightly broader central profile than the quasar.

For all of the quasars modelled, the total light within the eight extra psf components was not found to be systematically positive or negative. If adding 8 extra ‘psf components’ around the core had always resulted in a total positive (or negative) component being subtracted from the quasar, this would have suggested that either these components were removing host light in addition to ‘leaking’ nuclear light, and that the host profile breaks down in a systematic way for these pixels, or that our observing strategy had produced a systematically incorrect psf.

For all quasar host galaxy studies, there is no escap-

psf cmpts	$R_{1/2}$ /kpc	L_{int} /adu	a/b	α	β	χ^2
1	10.45	312.7	0.61	1.05	0.77	2840.3
9	9.76	350.1	0.64	1.04	0.92	2814.2
25	9.71	353.3	0.65	1.03	0.93	2799.9

Table 2. Recovered host galaxy parameters for quasar 0956–073 modelled using different numbers of additive psf components.

ing the fundamental problem that the galaxy profile has to extrapolated into the central region from some radius (to separate host and nuclear light). By adding in these extra components, all we’re doing is extrapolating from different distances, and arguing that simply extrapolating only into the central pixel is not necessarily correct for these data. This is because the measured psf is incorrect for the (discrete) deconvolution problem we’re trying to solve.

6.3 The error frame

Determining the fit between model and image requires an estimate of the relative noise in each pixel, from both intrinsic noise in the image and differences between measured and true psf. Ideally these errors should be estimated without recourse to the images but, unfortunately, this is impractical for these data. Faced with a similar problem, Taylor *et al.* (1996) estimated the radial error profile by measuring the error in circular annuli of the image from which a multiple of the psf had been subtracted centred on the quasar with matched total luminosity. Using both the image and measured psf in this way allows the error from psf differences to be included in the error frame. However, this model assumes that the host galaxies do not introduce any intrinsic variations in the annuli within which the variance is calculated. Such variations could result from either differences between the radial profile of the host (convolved with the psf) and the psf profile, or significant deviation from circular host profiles. These effects will be small because the hosts only contribute a small percentage of the light and deviations from circular hosts are small.

In order to reduce the number of parameters required to calculate the error profile and hopefully alleviate any damage caused by calculating the error frame from the data, Taylor *et al.* (1996) showed that a function of the form $\log(\sigma_i) = A \exp^{-0.5(r/S)^\gamma} - B$, where A,B,S and γ are four parameters, provides a good fit to the resulting profile. This profile models both the error in the central regions of the image and the Poisson background error outside the core. The four parameters are determined for each quasar by least-square fitting to the observed error profile. Such a fitting procedure also enables the error to be determined in the central regions where the gradient is too steep and there are too few points in each annulus to predict confidently the error. In general this function fits the observed error profiles very well, and is used here (without including a contribution from the host) to estimate the errors in each pixel.

Fig. 3 shows the observed and fitted error profiles for quasars 0956–073 and 1543+489 with and without including the best-fit model galaxy in the analysis. The best-fit host around quasar 1543+489 has an axial ratio of 0.89 in

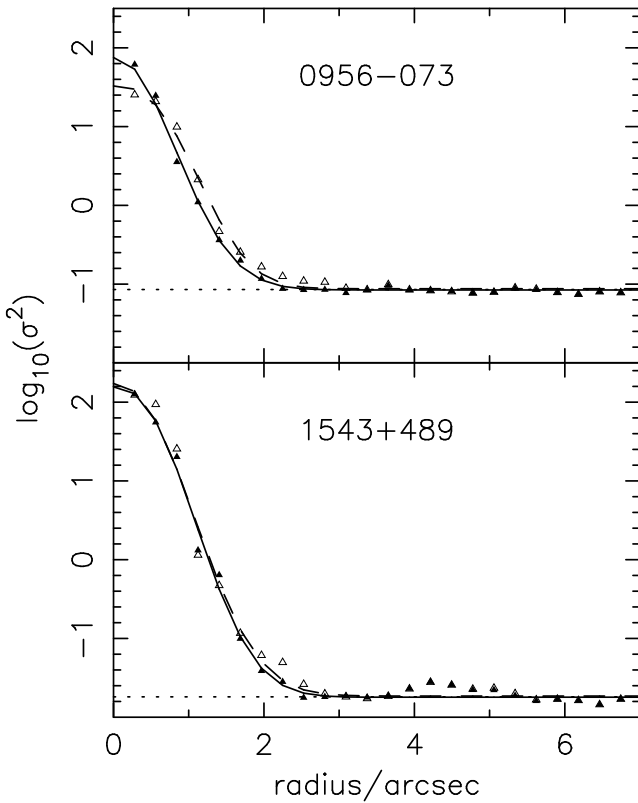


Figure 3. The calculated radial profile of the variance measured in annuli of width 0.3 arcsec of the difference between the image of the quasar and the scaled psf (open triangles). The best-fit model for this profile calculated as in Section 6.3 is also plotted (dashed line). For comparison the radial profile, calculated in the same way, for the difference between the image and best-fit model galaxy with one nuclear component is plotted (solid triangles) and the model of this profile (solid line). This solid line shows the radial error profile used to produce the simulated data of Section 9. The dotted line shows the Poisson noise level of the sky background. Top panel: quasar 0956–073, bottom panel: quasar 1543+489.

contrast to 0.64 for 0956–073. The deviation of the host around 0956–073 from circular symmetry explains why the error profile changes when including this host more than for quasar 1543+489.

6.4 χ^2 minimisation

The algorithm used to find the global minimum in χ^2 was a multi-dimensional direction set technique based on a method introduced by Powell in 1964 (Press *et al.* 1992). This algorithm requires an initial ‘start point’ from which it works its way downwards until it finds the minimum position. Briefly, the algorithm minimises χ^2 by sequentially adjusting each parameter (i.e. minimising along the axes of the parameter space), and then it minimises χ^2 on the vector along which the greatest change was made to χ^2 in the previous steps. This procedure is repeated until the algorithm converges. Additionally, for all the quasars it was ascertained that the algorithm had found the correct minimum and not erroneously finished early due to a numerical convergence problem by repeatedly re-running the algorithm starting from

the previous best-fit parameters until the total host luminosity found for successive runs differed by less than 0.1 adu. The testing performed for this algorithm is described in Section 7.2.

For all the results presented in Section 8, the algorithm was started from an initial position in parameter space corresponding to a broad, low luminosity galaxy. This was chosen so the algorithm avoided straying into a region of parameter space where all of the host light was in the core (i.e. small $R_{1/2}$). This is a relatively flat region for χ^2 in parameter space and it can therefore take a long time for the algorithm to work its way out of this region.

All pixels within a radius of 31 pixels (8.7 arcsec) measured from the centre of the quasar were included in the calculation of χ^2 . For all of the best-fit host galaxies, the difference between model host luminosity within this area and the integrated luminosity was negligible, which implies that this area contained all of the important signal.

7 TESTING THE MODELLING PROCEDURE

7.1 Robustness to the error profile

As a test of the robustness of the best-fit host luminosities to the determination of the error profile, we have modelled our image of quasar 0956–073 using different error profiles. Quasar 0956–073 was chosen for this test because the derived axial ratio of the host is the lowest of any quasar (although the range of values is quite small: Section 8.3). If the galaxy is important in the error frame calculation, the error profile calculated for this quasar as in Section 6.3 should be the most affected by the fact that we are ignoring the host (see Fig. 3). Using an error profile calculated as in Section 6.3 but using the image only (i.e. not subtracting the psf), the integrated host brightness was found to drop from 350.1 adu to 316.6 adu, corresponding to a variation of ~ 0.1 mag. We have also tried re-calculating the error frame from the image minus the best-fit model image (galaxy and nuclear component convolved with the psf), again using the above formula to fit the error frame. Radial profiles of the two error frames are shown in Fig. 3. The best fit model parameters were used to calculate a new error frame, and we repeated this process until the best-fit host luminosity converged (subsequent iterations altered the integrated host luminosity by less than 0.1 adu). The final best-fit luminosity was found to be 351.5 adu, a negligible difference from the original minimum.

7.2 Finding the minima

Obvious tests to perform are that there is only one minimum for each quasar, and that the χ^2 function is well behaved around this point. Obviously, it is impossible to cover every position in parameter space to check that χ^2 is well-behaved and that there are no local minima. However, we have examined the region of parameter space of interest using a variety of techniques and have found no potential problems.

The minimisation algorithm is itself designed to cover a large region of parameter space; the algorithm sequentially searches for the minimum along a series of vectors (see Section 6.4 for details), and considers a large number of diverse

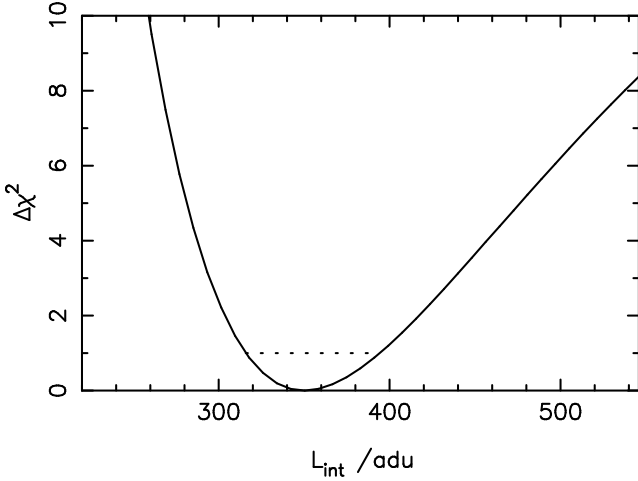


Figure 4. The variation of χ^2 (normalised to the minimum value) versus fixed total host luminosity. For each point on the curve, all parameters other than the luminosity have been altered to obtain the local minimum in χ^2 . The 68.3% confidence interval, found by a separate binary search is also shown (dotted line).

values along each vector. Rerunning the algorithm starting at the best-fit location previously found also tests any minimum along each axis in parameter space, as does the calculation of the error bars, described in Section 7.4. The shapes of the surfaces around each minimum are also revealed by this calculation.

A test for local minima has been performed for quasar 0956–073 over a larger region of parameter space: the minimisation algorithm was started at a large number of diverse initial host parameters, and no significant change in the best-fit parameters was discovered. Quasar 0956–073 was chosen for this test because it has average signal-to-noise of any quasar. Fig. 4 shows a ‘slice’ through parameter space revealing how smoothly the constrained χ^2 minimum varies with fixed host luminosity for quasar 0956–073. To calculate each point of this curve, all of the parameters except the host luminosity were varied until the constrained χ^2 minimum was reached. The remarkable smoothness of this curve demonstrates both that the global minimum is well pronounced and the function varies smoothly towards it, and that the minimisation routine is finding the correct minimum at each point: if it were not, a more rough surface would be expected, signifying that the optimum position had not been reached for each host luminosity.

7.3 Using the χ^2 statistic

Use of the χ^2 statistic is dependent on the error in each pixel being independent of the errors in the other pixels. This is expected if the errors in the images are dominated by Poisson shot noise. Any large-scale differences between actual and model host could provide correlated errors, although these would hopefully have been discovered by the analysis of Section 5. It is possible that small-scale discrepancies remain that extend across more than one pixel. However, the relatively large pixel scale works to our advantage by reducing the likelihood of this. The central limit theorem then

suggests that the error in each pixel should have approximately Gaussian distribution.

The minimum χ^2 values are highly dependent on the normalisation of the error frames, and cannot directly provide tests of the model fits. The position of these minima are unaffected by the normalisation of the error frame as they are only dependent on relative variations between pixels. Examining the reduced χ^2 values at the minima given in Table 4, we see that the reduced χ^2 is less than 1 for the majority of the quasars, and deduce that the procedure outlined in Section 6.3 slightly over-estimates the error in each pixel. This is as expected due to the effect of the host galaxy. The confidence intervals calculated in Section 7.4 will therefore be slightly too large, thus providing a moderately pessimistic error analysis.

As any nearby companions were excluded when measuring χ^2 , the number of pixels used, presented in Table 4, varies between quasars. For quasar 1214+180, a diffraction spike from a nearby star which ran close to the quasar was also excluded. Unfortunately the position of the pixels which were not modelled is more important than the number of such pixels and, for this quasar the position of the diffraction spike was such that it covered a highly important region of pixels. Even though the area covered was small, the modelling suffered greatly.

7.4 Calculating error bars on the parameters

Provided that the galaxy model is a good representation of the true underlying host galaxy, the errors between the model and image are uncorrelated between separate pixels, and the procedure in Section 6.3 provides approximately the correct error frame (see Section 7.3), it is possible to calculate error bars on the true parameters using the χ^2 statistic. The procedure to do this is to hold the chosen parameter fixed at a certain value, and minimise the remaining parameters to find the local minimum in χ^2 . The end points of the 68.3% confidence intervals on the best-fit parameter are given by the points for which $\Delta\chi^2 = \chi^2 - \chi_{\min}^2 = 1$, where χ_{\min}^2 is the minimum value calculated allowing all parameters to vary (Bevington & Robinson 1992). A standard binary search has been used to find the required limits. As well as allowing error bars to be calculated, this procedure enables the parameter space to be examined and any problems for each quasar to be spotted.

In order to match the light from the host galaxies, the behaviour of the integrated host luminosity, β and $R_{1/2}$ are coupled (Abraham, Crawford & McHardy 1992). The determination of the error bars is therefore complicated by the question ‘what limits, if any should be placed on the parameters being adjusted to find the constrained minima?’ In finding the global minima, all of the parameters are effectively allowed to vary over all space: although bounds are placed on the parameters, they are not reached (except when modelling the star, see Section 7.5). However, at fixed integrated host luminosity, these limits are often reached because the profiles required to optimally match the light do not necessarily have to be those of galaxies. The philosophy adopted is that all the parameters should be allowed to vary except β , upon which limits of $0.25 < \beta < 6.0$ should be set to provide some adherence to standard galaxy profiles.

For quasar 0956–073, we have examined the required

cut through parameter space for the integrated host luminosity, calculated by minimising all other parameters to obtain each point. The distribution of local χ^2 minima are shown in Fig. 4: the curve displays simple structure, monotonically decreasing to the global minimum from both directions so we are justified in using the simple $\Delta\chi^2 = 1$ cut-off for the error bars. The resulting 68.3% confidence interval for the luminosity is also shown.

The value of χ^2 depends on the error frame used, and it is expected that the error bars do so as well. The effect of altering the error frame for quasar 0956–073 has been tested by using the error frame calculated from the image only as in Section 6.3. Using this error frame, the 68.3% confidence interval on the host magnitude changed slightly from $-25.11 < M_K < -24.87$ to $-25.10 < M_K < -24.66$.

7.5 Fitting to a normal star

On the same frame as quasar 0043+039 we observed a star of similar signal-to-noise as the quasar. As a test of the fitting procedure we decided to see if we could fit a ‘galaxy’ to the star. Starting from an initial position in parameter space corresponding to a broad, low luminosity galaxy as adopted in all of the modelling, the resulting best-fit parameters are given in Table 3. As can be seen, the fitting procedure rolled down the hill towards a host galaxy of very low luminosity. At such low total luminosity, the remaining four galaxy parameters are poorly determined: altering these parameters results in a very small change in χ^2 . Consequently it is no surprise to find that the best-fit $\beta = 6$ value is one of the limits set in the modelling procedure.

8 RESULTS OF THE ANALYSIS

8.1 Luminosities

For three of the quasars, analysis of how χ^2 varies within the parameter space revealed that the best-fit host luminosity was not well constrained. A host galaxy was determined as being present in that a lower limit was determined in all cases. However, the maximum light which could have come from the host was not clear because the shape of the host was not sufficiently resolved. The morphology of the best-fit galaxy at large L_{int} could alter to place the majority of the host light in the central region. This effect could have been avoided by placing limits on $R_{1/2}$ or, for instance, using the near-infrared Fundamental Plane (Pahre, Djorgovski & de Carvalho 1998), although these upper limits would have been highly dependent on the criteria set. The host luminosity is ultimately limited by the total light in the image, and it is expected that the host luminosities for these quasars do have upper bounds at high values of L_{int} , but these high values would not be of any use in determining the actual host light.

For the remaining nine quasars, the minima were sufficiently constrained to provide 68.3% confidence intervals. Comparison of different confidence intervals provided information on the depth of the valleys within which each minimum was found and the quality of each determination.

Host and nuclear luminosities for our quasars are compared with the results of other studies in Fig. 5. In order to

compare with the H -band host galaxy studies undertaken by McLeod & Rieke (1994a;b), we convert their total (nuclear + host) and host luminosities to the K -band by applying a single conversion factor to the apparent magnitudes. This then sets the relative normalisation of the K -band and H -band samples; conversion to absolute magnitudes is subsequently undertaken in exactly the same way for all of the infra-red samples.

In a study of the energy distribution of the PG quasars (from which McLeod & Rieke chose their samples), Neugebauer *et al.* (1987) found $\langle H - K \rangle = 0.90$ for the sample of McLeod & Rieke (1994a) and $\langle H - K \rangle = 0.98$ for McLeod & Rieke (1994b). In the upper panel of Fig. 5, we adopt these values to convert the total luminosities of the McLeod & Rieke quasars into the K -band.

The light from the galaxy component is assumed to be dominated by an evolved stellar population, the colour of which reddens with increasing redshift. For nearby galaxies, $H - K \sim 0.25$, which was used by McLeod & Rieke (1995) to convert galaxy absolute magnitudes. However, the apparent $H - K$ is dependent on redshift and, at the redshifts of the quasars imaged by McLeod & Rieke (1994a;b), $H - K \sim 0.6$ is expected for an evolved stellar population (Lilly & Longair 1984). This was adopted to convert the McLeod & Rieke galaxy luminosities into the K -band.

We have also checked the calibration of the McLeod & Rieke samples and our sample of modelled quasars (with 6 overlapping objects) against the data of Neugebauer *et al.* (1987). The average total quasar luminosity for the subsamples are in good agreement, although individual values vary by up to 0.7 mag, presumably due to intrinsic quasar variability.

One quasar (1354+213) was imaged by McLeod & Rieke (1994b), Neugebauer *et al.* (1987) and in our study. Neugebauer *et al.* (1987) derived $H - K = 1.0$ for this object, which is higher than $H - K = 0.3$ derived by combining the McLeod & Rieke H -band and our K -band observation. However, the McLeod & Rieke and our observations were undertaken at different epochs, and the luminosity is not expected to remain constant.

The study of Taylor *et al.* (1996) was performed in the K -band, and the apparent K -band magnitudes of host and nuclear components were taken directly from this work. The data from the different infra-red samples were then converted to absolute magnitudes, applying the K -correction of Glazebrook *et al.* (1995) for the host galaxy and assuming the nuclear component follows a standard power law spectrum $f(\nu) = \nu^{-0.5}$.

Using the error bars calculated in Section 7.4 to weight the data, the average integrated host galaxy magnitude for our quasars was found to be $\langle M_K \rangle = -25.15 \pm 0.04$. For comparison, when converted for cosmology exactly as our data, the sample of Taylor *et al.* (1996) gives $\langle M_K \rangle = -25.68$, McLeod & Rieke (1994a) $\langle M_K \rangle = -25.42$ and McLeod & Rieke (1994b) $\langle M_K \rangle = -25.68$.

Recent determinations of the K -band luminosity of an L^* galaxy (Gardner *et al.* 1997) have resulted in $M_K^* = -24.6$, compared to previous determinations of $M_K^* = -24.3$ (Glazebrook *et al.* 1995) and $M_K^* = -25.1$ (Mobasher, Sharples & Ellis 1993). The Gardner *et al.* (1997) value is plotted in the top panel of Fig. 5. This shows that the average luminosity of our hosts is ~ 1.6 times that of an L^*

quasar	$R_{1/2}$ /kpc	L_{int} /adu	axial ratio	α /radians	β	nuc/host ratio	K_{host}	K_{tot}	K_{psf}
0043+039	7.41	355.0	0.96	1.44	0.60	13.9	16.04	13.54	11.90
0137-010	5.09	407.5	0.66	2.55	2.05	13.7	15.96	13.46	10.83
0244-012	3.28	165.6	0.86	2.66	0.61	16.6	16.87	14.18	11.15
0316-346	8.56	864.8	0.76	0.07	1.25	12.2	15.15	12.73	9.62
0956-073	9.76	350.1	0.64	1.04	0.92	21.4	16.02	13.07	9.20
1214+180	3.24	259.7	0.74	1.25	1.12	15.2	16.34	13.75	8.52
1216+069	19.75	379.3	0.74	2.42	2.73	21.4	15.93	12.99	11.10
1354+213	11.55	481.4	0.69	1.38	0.73	6.79	15.67	13.82	9.21
1543+489	7.75	320.1	0.89	3.00	0.67	25.9	16.12	12.98	9.92
1636+384	-	-	-	-	-	24.1	17.65	14.11	10.07
1700+518	-	-	-	-	-	14.8	15.86	11.82	10.23
2112+059	5.59	169.1	0.93	0.49	2.13	67.0	16.85	12.72	11.08
2233+134	8.01	175.0	0.80	1.54	0.64	28.5	16.88	13.64	10.17
2245+004	5.16	572.9	0.81	1.93	3.16	1.25	15.52	14.87	10.02
star	16.6	0.000031	0.16	2.26	6.0	-	-	-	-

Table 3. Best-fit host galaxy parameters as determined by the 2D modelling described in Section 6. Also included for comparison are the best-fit parameters for a nearby star found on the frame of quasar 0043+039 which had similar signal to noise as the quasar. For quasars 1636+384 and 1700+518 deconvolution of the images revealed a highly disturbed morphology which extended close to the core of the quasar and model fitting was not attempted. Consequently host galaxy magnitudes presented for these quasars are the relatively inaccurate measurements calculated from the deconvolved images as described in Section 5. Nuclear-to-host ratios are calculated in the rest frame of the quasar from the derived absolute magnitudes in order that these values are consistent with Fig. 5 (see Section 8.1 for details). The apparent magnitudes of the quasar, the host component, and the star used to give a psf measurement are also presented.

quasar	χ^2	number of pixels modelled	reduced χ^2	min	L_{int} /adu best-fit	max	min	M_K (host) best-fit	M_K (tot)	
0043+039	2639.79	2885	0.92	287.7	355.0	454.4	-25.56	-25.29	-25.07	-28.22
0137-010	2661.25	2987	0.89	333.7	407.5	-	-25.08	-24.87	-28.01	
0244-012	2985.64	2974	1.00	63.9	165.6	999.4	-26.85	-24.90	-23.86	-28.01
0316-346	2674.08	2987	0.90	766.3	864.8	1009.7	-25.61	-25.44	-25.31	-28.24
0956-073	2814.17	2987	0.94	315.8	350.1	394.4	-25.11	-24.98	-24.87	-28.36
1214+180	2499.93	2509	1.00	112.7	259.7	-	-24.94	-24.03	-27.96	
1216+069	2437.36	2625	0.93	290.2	379.3	604.0	-25.62	-25.11	-24.82	-28.49
1354+213	2281.14	2987	0.76	462.4	481.4	502.1	-25.20	-25.16	-25.11	-27.38
1543+489	2567.80	2874	0.89	263.6	320.1	402.3	-25.56	-25.31	-25.10	-28.89
2112+059	2876.00	2945	0.98	37.7	169.1	-	-24.91	-23.29	-29.50	
2233+134	2679.73	2941	0.91	108.7	175.0	269.2	-24.58	-24.11	-23.59	-27.78
2245+004	2584.98	2987	0.87	438.1	572.9	941.6	-26.24	-25.70	-25.41	-26.48
star	3055.42	2969	1.03	-	0.000031	-	-	-	-	

Table 4. Table showing the end points of the 68.3% confidence intervals calculated as in Section 7.4 for the best-fit integrated host luminosities. To further aid comparison between model fits for different quasars, the χ^2 values for the best fit model are presented with the number of pixels used in this calculation. Note that the position of the un-modelled pixels is more important than the number of such pixels.

galaxy. Note that for all three values, the derived average luminosity is 1–2 times that of an L^* galaxy, and the conclusions of Section 11.1 are not affected by this choice.

We compare our sample to recent HST R -band results in the lower panel of Fig. 5 assuming an apparent $R - K = 2.5$ for the total light from our quasars based on the average value for the 6 quasars which overlap our sample and the sample of Neugebauer *et al.* (1987). The $R - K$ colour of an evolved stellar population, assumed to dominate the host galaxies, is dependent on the redshift of the source and, for the redshifts of our sample ($z \sim 0.35$), is expected to be ~ 3.5 (Dunlop *et al.* 1989). All the data (including our data after conversion to apparent R -band magnitudes) presented in the bottom panel of Fig. 5 were adjusted for cosmology assuming that the nuclear component has a spectrum of the

form $f(\nu) \propto \nu^{-0.5}$, and the galaxy component has $f(\nu) \propto \nu^{-1.5}$.

8.2 Morphologies

Morphologies are parametrised by the best-fit value of β : $\beta = 1$ values correspond to disk-like, and $\beta = 4$ to spheroidal profiles. The technique described in Section 7.4 has been used to reveal how well the β parameter is constrained by the modelling. The result of this analysis is presented in Table 5. As can be seen, the β parameter is well constrained for fewer quasars than the luminosity and χ^2 error bars reveal a highly skewed distribution for the expected true value given the best-fit β value. In order to correctly determine the differential probability between disk and spheroidal profiles, we

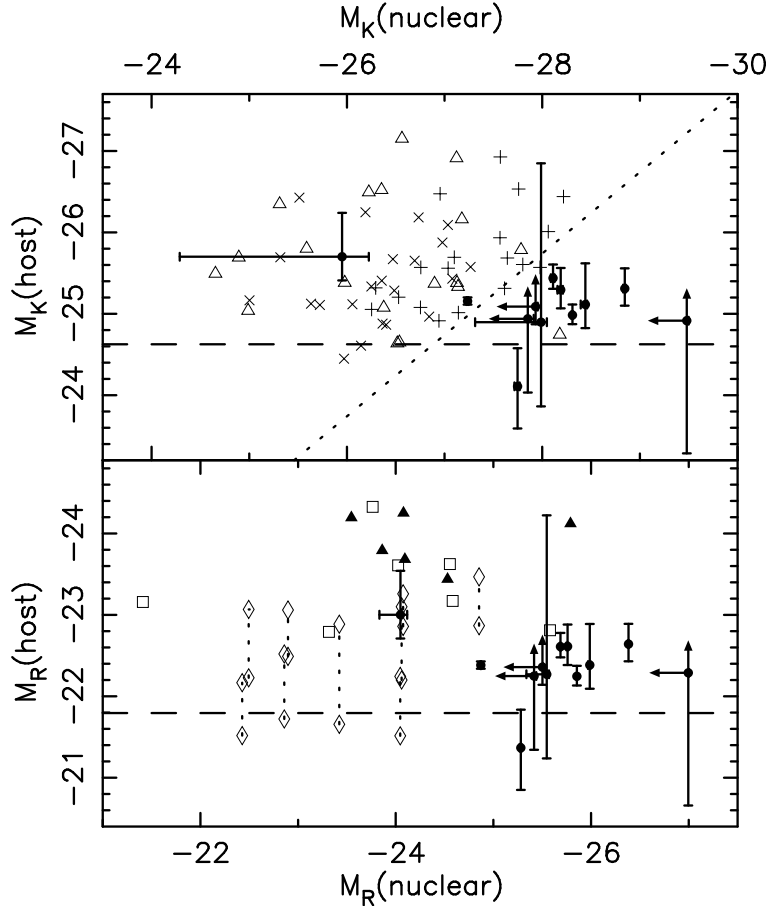


Figure 5. The top panel shows nuclear vs. integrated host absolute K -band magnitudes for our sample of quasars (solid circles) with error bars calculated as described in Section 7.4. The errors in the measured nuclear component are derived from these and consequently the errors are strongly correlated. Plotted for comparison are the calculated host magnitudes for the radio-quiet quasars imaged by Taylor *et al.* (1996) (open triangles), McLeod & Rieke (1994a) (crosses) and McLeod & Rieke (1994b) (plus symbols). Details of the conversion of the McLeod & Rieke data from the H -band to the K -band can be found in Section 8.1. The luminosity of an L^* galaxy, $M_K^* = -24.6$ (Gardner *et al.* 1997) is also plotted (dashed line), as is the locus of points with a rest-frame K -band nuclear-to-host ratio of 8 (dotted line). In order to compare with recent HST results, in the bottom panel we convert our data into the R -band (see Section 8.1 for details). Symbols for our data are as for the top panel. The R -band best-fit luminosities from disk or exponential galaxies (Hooper, Impey & Foltz 1997) are also plotted (diamonds separated by dotted lines). No attempts were made to distinguish the best host morphology in this work. The derived R -band host luminosities of McLure *et al.* (1999) are also shown (radio-quiet sample: open squares, radio-loud sample: solid triangles). The luminosity of an L^* galaxy, $M_R^* = -21.8$ (Lin *et al.* 1996) is plotted for comparison (dashed line).

need to know the relative dispersion of β for each morphological type. However, examining the best-fit parameters, the error bars on β , and the shape of χ^2 surface, on which we have information from the binary search to find the error bars, we can infer the best fit morphology for some of the quasars. The suggestion from this is that luminous radio-quiet quasars can exist in hosts dominated by either disk-like or spheroidal components. A histogram of these data is plotted in Fig. 8, where the distribution is compared to that recovered from simulated data with exact $\beta = 1$ or $\beta = 4$ profiles.

8.3 Axial ratios and angles

Analysis of the parameter space reveals that the axial ratio and projected angle of each host are better constrained than the other parameters. Fig. 6 shows histograms of these parameters for all quasars modelled. The distribution of axial

ratios is small with $\langle a/b \rangle = 0.79 \pm 0.03$. This is in agreement with those found by McLure *et al.* (1999), but higher than found by Hooper, Impey & Foltz (1997). The projected angles are uniformly distributed as expected.

8.4 Highlighted results for selected quasars

8.4.1 Quasar 0043+039

The broad-absorption-line (BAL) quasar PG0043+039 has been subject to 2 previous studies to determine host galaxy properties. It was observed in the i band by Veron-Cetty & Woltjer (1990) who determined $M_i = -23.9$ if the host is a disk like ($\beta = 1$) galaxy, or $M_i = -24.7$ for a spheroidal ($\beta = 4$) galaxy. This quasar was also observed using the wide-field camera on HST by Boyce *et al.* (1998), who used a cross correlation technique to determine that the host was slightly better fit by a disk galaxy with $M_V = -21.6$. We

quasar	min β	β	max β	morphology?
0043+039	0.42	0.60	0.86	disk
0137-010	1.52	2.05	>6.0	spheroid
0244-012	<0.25	0.61	1.62	disk
0316-346	1.02	1.25	3.62	?
0956-073	0.71	0.92	1.21	disk
1214+180	<0.25	1.12	>6.0	?
1216+069	1.44	2.73	>6.0	spheroid
1354+213	0.65	0.73	0.82	disk
1543+489	0.49	0.67	0.90	disk
2112+059	<0.25	2.13	>6.0	?
2233+134	<0.25	0.64	1.21	disk
2245+004	2.17	3.16	5.55	spheroid

Table 5. Table showing 68.3% confidence intervals for the best-fit host β parameters for the 12 quasars modelled using the 2D χ^2 minimising technique (Section 6). Error bars were calculated as described in Section 7.4 with β constrained to lie in the range $0.25 < \beta < 6.0$. The morphology of the dominant contribution to the host galaxy is also presented, based on the best fit β parameter and associated confidence interval.

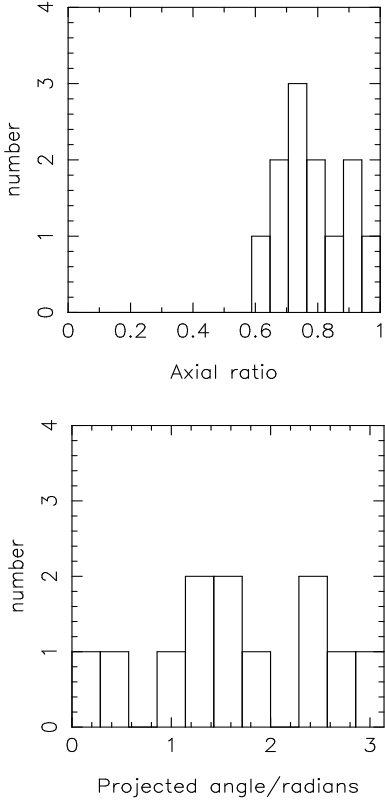


Figure 6. Histograms showing the distribution of axial ratios and projected angles of the host galaxies. These parameters were well constrained for all of the 12 quasars modelled, and are therefore plotted from all of the minima found. Axial ratios are tightly constrained with $a/b > 0.64$ for all hosts, and $\langle a/b \rangle = 0.79 \pm 0.03$. The distribution of projected angles is approximately uniformly distributed.

also find that the dominant morphology is disk-like and calculate $M_K = -25.29$. The old burst model of Bruzual & Charlot (1993) predicts $V - K = 3.3$ which is consistent with the derived $V - K = 3.7$.

8.4.2 Quasar 0316-346

This quasar was previously observed using the wide field camera on HST (Bahcall *et al.* 1997) and the host was found to reveal evidence of a merger, in particular tidal tails extending ~ 20 kpc west of the quasar. Bahcall *et al.* (1997) also provide a 2D fit to the host properties and find that the best-fit host is disk galaxy with $M_V = -22.3$. We also calculate a best-fit disk galaxy and find $M_K = -25.44$, giving $V - K = 3.1$, again consistent with the old burst model of Bruzual & Charlot (1993) which predicts $V - K = 3.3$.

8.4.3 Quasar 1214+180

There have been no previous attempts to determine the morphology of the host galaxy around this quasar possibly due to the nearby star which was utilised in this work to obtain an accurate psf. Unfortunately in our images, a diffraction spike from this star passed close to the quasar reducing the area that could be used to calculate χ^2 . Although the modelling converged to give basic galaxy parameters, further analysis of the parameter space revealed that this minimum was not well constrained.

8.4.4 Quasar 1216+069

Our analysis of this quasar benefited because the images were obtained using the tip-tilt system and there is a nearby bright star which was placed on the same frame as the quasar and used to obtain a psf measurement. Previously, ‘nebulosity’ has been observed around this quasar (Hutchings, Crampton & Campbell 1984), and a more detailed HST study found a best-fit spheroidal ($\beta = 4$) galaxy with $M_V = -22.3$ (Boyce *et al.* 1998). We also find that the most likely host is a large spheroidal galaxy and obtain $M_K = -25.1$, giving $V - K = 2.8$.

8.4.5 Quasar 1354+213

Using a psf subtraction technique, McLeod & Rieke (1994b) found a residual host galaxy with $M_K = -25.6$ when converted to our cosmology using the K -correction from Glazebrook *et al.* (1995) and the apparent colour correction $H - K = 0.6$ (see Section 8.1). Our best fit host luminosity was $M_K = -25.2$. Analysis shows that the luminosity and the β parameter are both tightly constrained by the modelling and the best-fit $\beta = 0.73$ suggests that the host is dominated by a disk component. The rest-frame nuclear-to-host ratio for this quasar is only 6.8 (the apparent nuclear-to-host ratio is 4.6), which explains why the derived parameters have small error bars.

8.4.6 Quasar 1636+384

We are not aware of any previous attempts to determine the luminosity and morphology for the host galaxy of quasar

1636+384. Preliminary deconvolution of the light revealed that the excess, non-central light displayed a morphology greatly disturbed from elliptical symmetry (as shown in Fig. 2). The structure includes an excess of light to the NW of the core which is interpreted as a merging component as well as light around the central core which probably originates from the host. From this image it was unclear how to distinguish between the host and the interacting companion, so the luminosity of the host was estimated by summing pixel values excluding the central pixel. This provided an approximate K -band absolute magnitude of $M_K = -23.5$.

8.4.7 Quasar 1700+518

Quasar 1700+518 is a bright BAL quasar of low redshift ($z = 0.29$). Such low redshift BAL objects are rare and hard to discover since the broad absorption lines are in the UV and consequently quasar 1700+518 has received much interest: specific studies of this quasar have been undertaken in many different wavebands (Hutchings, Neff & Gower 1992; Stockton, Canalizo & Close 1998; Hines *et al.* 1999). Because of the low redshift and the brightness of the quasar, 1700+518 has also been included in many samples of quasars imaged to obtain details of their host galaxies (Neugebauer *et al.* 1985; McLeod & Rieke 1994b), although these have only provided upper limits for the host magnitude. More recent imaging studies have shown that the morphology of the underlying structure consists of a disturbed host predominantly to the SW of the core (Stockton, Canalizo & Close 1998) and a close interacting companion to the NE (Hutchings, Neff & Gower 1992) which is most likely a ring galaxy (Hines *et al.* 1999). Deconvolution of the light from this quasar, as shown in Fig. 2, confirms this picture of the structure. With the disturbed morphology it is difficult to know how to split the light in the central pixels into nuclear and host components. As for quasar 1636+384 the host luminosity was estimated by summing the counts in the pixels surrounding the central one (ignoring those from the NE companion). There will be errors caused by leakage of light from the nuclear component and from the contribution of the host to the central pixel. An approximate K -band absolute magnitude of -24.9 was obtained for the host galaxy and -24.4 for the NE companion galaxy.

8.4.8 Quasar 2233+134

Both Smith *et al.* (1986) and Veron-Cetty & Woltjer (1990) included this quasar in their samples, but both failed to resolve the host galaxy beyond obtaining upper limits for the luminosity. Hutchings & Neff (1992) did resolve the host galaxy and found the host to be best-fit by a $\beta = 4$ model, although they did not resolve further information about the galaxy. However, we find that the most probable host has an disk profile and calculate $M_K = -24.1$, the lowest luminosity host modelled. If we constrain the host to have an elliptical profile, the best fit luminosity becomes $M_K = -25.9$, although the half light radius is very small for this model ($R_{1/2} = 1.5$ kpc) which places it a long way from the K -band Fundamental Plane of Pahre, Djorgovski & de Carvalho (1998). If the host parameters are constrained to lie on this plane, then rerunning the modelling gives a best fit

host with $M_K = -24.6$. Neither of these changes would be sufficient to alter our conclusions.

9 SIMULATED DATA I - SINGLE COMPONENT GALAXIES

Trying to recover known host parameters from Monte-Carlo simulations of the actual data enables the distribution of recovered parameters given the true values to be determined. Note that the error bars calculated using the χ^2 statistic are instead determined from the distribution of possible true values given the data. These two distributions are not necessarily equal. We need to determine the distribution of recovered values in order to answer questions such as ‘Are our results biased towards low β values?’.

In view of the distribution of recovered β values, it was decided to simulate data to match the images of quasars 0956–073 and 1543+489. These quasars span the distribution of signal-to-noise of all the images, and 2D model fitting revealed evidence for disk dominated hosts in both cases. Verification of this result is interesting as recent work has suggested that the hosts of luminous quasars should be dominated by the spheroidal component (see Section 11.2).

9.1 Creating the mock data

Simulated galaxies were created using the procedure outlined in Section 6.1 and a single δ function added to the centre of each to create a ‘perfect unconvolved model’. The height of the δ function was chosen to match the total signal of the original images. These models were then convolved with the psf measured to match the quasar.

Gaussian noise was added with a radially dependent variance as given by the error profile calculated in Section 6.3 including the best-fit host galaxy in the calculation. The error profiles used for quasars 0956–073 and 1543+489 are given by the solid lines in Fig. 3. Differences between measured and true psf were included in this analysis, and are therefore included in the noise levels added to the simulated data. This noise model assumes that the errors in different pixels are independent (see Section 7.3).

We have simulated 100 images with exact disk hosts, and 100 images with exact spheroidal hosts for each of the two quasars chosen. The true integrated host luminosity was set at 300 adu for simulated data of both quasars. This conservative value is below the best-fit value obtained from the data for both quasars, providing a stringent test of the modelling. This is particularly true for a $\beta = 4$ host: constraining $\beta = 4$ when modelling the observed image would have resulted in a best-fit $L_{\text{int}} \gg 300$ adu. The simulated images were analysed using exactly the same 2D modelling procedure described above for the observed data. The range of recovered parameters is analysed below.

9.2 Results from the simulated data: luminosities

Recovered luminosities, presented in Fig. 7 reveal a skewed distribution, particularly for hosts with exact spheroidal profiles where the recovered luminosity is biased towards a low value. This is consistent with the morphology being skewed towards a low β value (see next Section): if β is

quasar	true	β			true	$L_{\text{int}} / \text{adu}$		
		min	average	max		min	average	max
0956–073	1.0	0.74	1.14	2.28	300.0	262.1	323.7	510.0
0956–073	4.0	1.93	3.77	7.42	300.0	213.6	288.3	463.1
1543+489	1.0	0.79	1.08	1.69	300.0	260.1	324.7	512.2
1543+489	4.0	2.13	4.04	7.25	300.0	209.6	302.2	469.8

Table 6. Table showing the mean and 68.3% confidence intervals for the recovered β and integrated host luminosity from the simulated data. 100 simulations were performed for each morphology for each quasar.

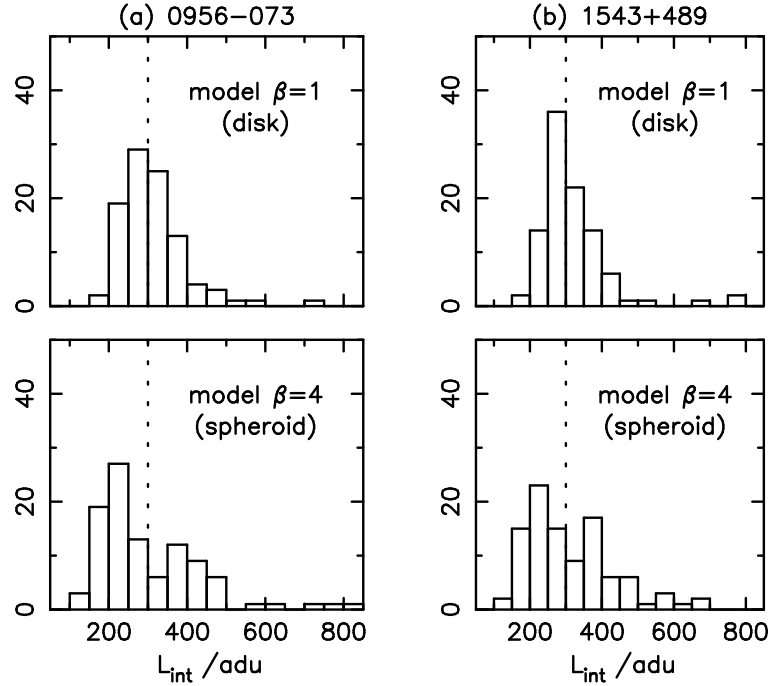


Figure 7. The distribution of recovered luminosities from Monte-Carlo simulations of 100 $\beta = 1$ images and 100 $\beta = 4$ images. The y -axis gives the number of recovered values within each luminosity bin. Noise has been added to match observations of quasar (a) 0956–073 and (b) 1543+489, including a contribution from the error in the measured psf as described in Section 9.1. The luminosity of each simulated galaxy, marked by the dotted line, was set at 300 adu.

decreased, the luminosity also has to decrease to keep the counts in the outer pixels (those most important for fitting the host) the same. The counts in the centre of the galaxy are less important because of the additional nuclear component which is adjusted to match the data.

The mean and variance in the recovered luminosities are presented in Table 6. Although the error bars reveal the extent of the skewed distribution, the mean is within 10% of the true value for each quasar and morphology.

9.3 Results from the simulated data: morphologies

The skewed distribution observed in the error bars on the true host β value is mirrored by the distribution of β values recovered using the standard modelling procedure described in Section 6. Fig. 8 shows the relative distribution of β values retrieved from the simulated images. Limits of $0.25 < \beta < 8$ were placed on fitted β values. For quasar 0956–073, 16 of the simulated images created with exact spheroidal hosts, had recovered $\beta > 8$. For quasar 1543+489, this number was

14: these values are not included in Fig. 8. The distribution was used to calculate the mean and standard deviation given in Table 6, assuming all fits with $\beta > 8$ actually had $\beta = 8$.

If the host were a spheroidal galaxy with $\beta = 4$, the probability of recovering a best-fit value of $\beta < 1$ is ~ 0.03 for 0956–073 and ~ 0.01 for 1543+489: the best-fit values from the images were $\beta = 0.92$ and $\beta = 0.67$ respectively. The evidence for the existence of hosts dominated by a disk component therefore appears to be strong. In Fig. 8, the distribution of retrieved β values for the 12 quasars modelled is also shown. This distribution is inconsistent with the hypothesis that all the hosts are dominated by spheroidal components on the scales probed by these measurements. The histogram is divided to show the probable distribution of morphologies given the options $\beta = 1$ or $\beta = 4$. As can be seen, the modelling suggests that approximately half of the hosts are dominated by disk components.

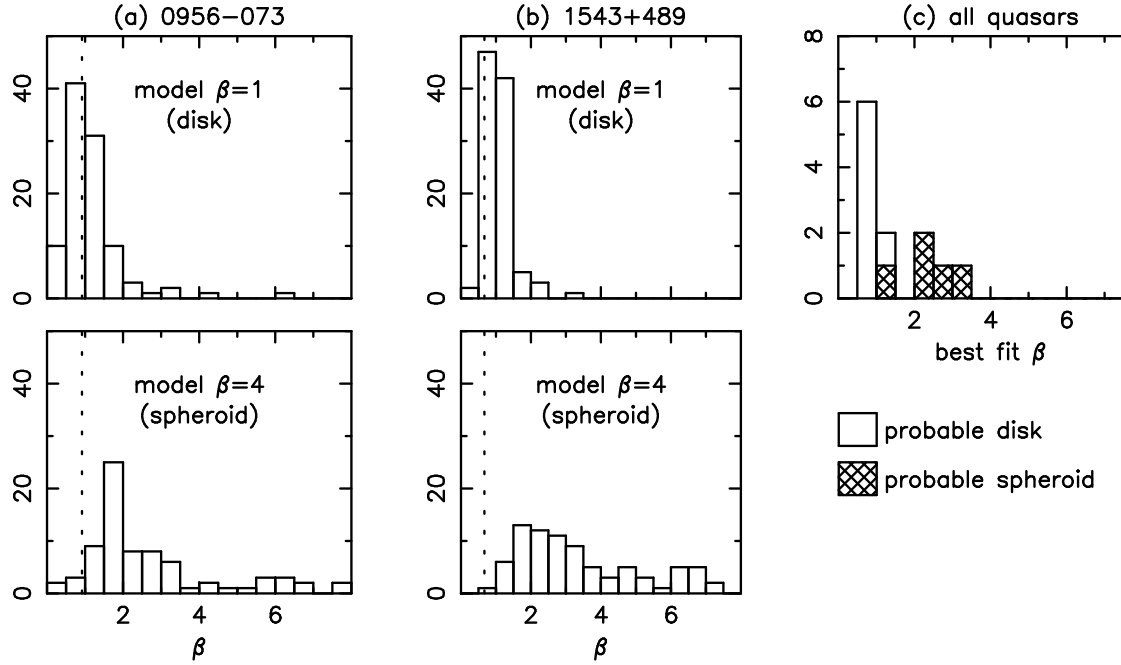


Figure 8. Evidence that the hosts of luminous radio-quiet quasars are not exclusively dominated by spheroidal components. The distribution of β values recovered from 2-D modelling of 100 simulated images created with hosts using exact disk or spheroidal profiles is presented. Noise has been added to these images to match observations of (a) quasar 0956–073 and (b) quasar 1543+489, including a contribution from the error in the measured psf as described in Section 9.1. The dotted line shows the best-fit β value recovered from the images of these quasars. (c) For comparison the distribution of best-fit β values obtained from all of our K -band images is also plotted. The probable morphology of the host was determined from the χ^2 error bars derived for the true value given the data.

10 SIMULATED DATA II - TWO COMPONENT GALAXIES

In order to constrain the potential importance of spheroidal cores in the galaxies found to be dominated by disk-like profiles, we have analysed synthetic quasars created with two host galaxy components. Using the Fundamental-Plane (FP) relation between $R_{1/2}$ and L_{int} found in the K -band by Pahre *et al.* (1998), we have added extra spheroidal ($\beta = 4$) components to the recovered best-fit host galaxy of quasar 1543+489. Note that this best fit host had $\beta = 0.67$. We have tried the same analysis using $\beta = 1$ and found no change in the effects produced by the spheroidal core. After adding in the nuclear component and noise as described in Section 9, we have recovered the best-fit host galaxy parameters using our single component modelling. Spheroidal components were added with a variety of different luminosities, and five different realisations of the additional noise component were added to each. The resulting average recovered L_{int} & β are given in Table 7.

Because $R_{1/2}$ (spheroidal) and L_{int} (spheroidal) follow a FP relation, the importance of this component is enhanced for large L_{int} (spheroidal) and diminished for small L_{int} (spheroidal). The recovered total luminosity for small spheroidal components is therefore very similar to that of the disk alone. For large spheroidal components, the modelling places an excess of host light in the core in order to simultaneously fit the outer disk-like profile and the inner profile with a single, large β value. This explains the behaviour of the difference between the actual and recovered L_{int} values. Recovered β monotonically increases with the increasing luminosity of the spheroidal core, suggesting that

spheroidal	L_{int} / adu			$R_{1/2}$ / kpc	β
	total	recovered	diff		
0.0	320.1	291.2	-28.9	8.26	0.61
40.0	360.1	306.5	-53.6	8.19	0.63
80.0	400.1	337.9	-62.2	8.02	0.69
120.0	440.1	382.7	-57.4	7.71	0.81
160.0	480.1	436.3	-43.8	7.35	0.96
320.0	640.1	785.8	145.7	5.45	1.93
480.0	800.1	1305.2	505.1	3.85	3.37

Table 7. Average recovered host parameters from single component fits to synthetic quasars with 2-component host galaxies. Uncorrelated Gaussian noise has been added to these models to match that of quasar 1543+489, and the average recovered values are given for 5 different realisations of this noise. The same noise was added to corresponding mock images created with different spheroidal luminosities, so there will be a systematic error because 5 realisations are not sufficient to fully sample the recovered parameters with the given noise level. The result of analysing a host with no spheroidal component shows that the results systematically underestimate β and L_{int} and overestimate $R_{1/2}$ by small amounts. Note that the relative dependence of the recovered parameters on the spheroidal component will not be affected.

the spheroidal core cannot be completely ‘hidden’ without affecting the best fit galaxy. This adds to the evidence that the low β values recovered for some of the quasars implies that they do not contain strong spheroidal components. Note that the recovered host luminosities are approximately correct for recovered values of β consistent with a host dominated by a disk-like profile.

For the quasars which have best-fit hosts dominated by spheroidal components, a disk-like profile at larger radii could have erroneously increased the recovered total host luminosity. However, in order to simultaneously fit these regions, small values of $R_{1/2}$ were required. For the quasars with hosts found to be dominated by spheroidal components, the relatively large values of $R_{1/2}$ recovered suggest that such a disk-like component is not present.

11 DISCUSSION

11.1 Luminosities

The integrated host luminosities derived from our K -band images exhibit a low dispersion around a mean similar to that calculated in studies of less luminous quasars. This is in accord with the work of McLure *et al.* (1999) who also found no evidence for an increasing trend, although they had fewer data points at high nuclear luminosity.

Previous HST studies have found evidence that host luminosity increases with nuclear luminosity (Hooper, Impey & Foltz 1997), although the trend observed in this work could be due to incorrect nuclear component removal: escaping nuclear light which increases in luminosity with the core could be added to the host light. It has recently been stated that the psf derived by packages such as TINYTIM, as used by Hooper, Impey & Foltz (1997) deviate from empirical WFPC 2 psfs at large radii (≥ 2 arcsec), due to scattering within the camera (McLure *et al.* 1999), and this could be the reason for an excess of nuclear light at larger radii which could be mistaken as host light. This excess light could also be the reason the low axial ratios observed in the Hooper, Impey & Foltz (1997) work are not in accord with those derived in McLure *et al.* (1999), or in this K -band study.

The triangular shape of the McLeod & Rieke points in Fig. 5 found for low redshift ($0 < z < 0.3$) Seyferts and quasars of lower luminosity than those in our sample, has been shown to be in accord with a lower limit to the host luminosity which increases with nuclear luminosity (McLeod & Rieke 1995). This cut-off in the host luminosity is equivalent to there being an upper limit to allowed nuclear-to-host ratios. The triangular shape is *not* followed by the results of the work presented in this paper which lie to the right of the McLeod & Rieke points. The relative positions of the two data sets in this Figure are set by the empirical $H - K$ corrections applied to the apparent H -band data (see Section 8.1 for details). Quasar 1354+213 was included in both our sample and the sample of McLeod & Rieke (1994b), and the results of both studies independently suggest a rest-frame nuclear-to-host ratio of 7 – 9. This places 1354+213 at the right of the triangular shape of the McLeod & Rieke points in Fig. 5, but it has a nuclear-to-host ratio lower than most of the quasars in our sample, and is therefore to the left of most of our points. We conclude that the limit suggested by McLeod & Rieke (1995) must break down for quasars with the highest nuclear luminosities.

This is in contrast to recent work by McLeod, Rieke & Storrie-Lombardi (1999) who claim that the lower bound on host luminosity extends to the highest luminosity quasars, partly based on the discovery of one luminous quasar, 1821+643 which appears to be in a host at $\sim 25L^*$. What

should we expect? The hosts of the quasars known to date already extend to about $2L^*$. Should the hosts of quasars which are ten times more luminous be found in galaxies at $20L^*$? Our analysis suggests not.

This result is highly important for recent quasar models. In particular, the model of Kauffmann & Haehnelt (1999) predicts that the upper limit to the nuclear-to-host ratio should extend to quasars such as those imaged in this work. However, this is clearly not the case. A possible fix to their model would be to invoke the scatter of the Magorrian *et al.* (1998) relations to explain high luminosity quasars (& high mass black holes) within low luminosity structures, and invoke a steeply-declining host mass function to explain the lack of really massive hosts. Further work on this model would then be required, particularly with regard to the revised slope of the high luminosity tail of the quasar luminosity function. Alternatively, factors other than black-hole mass, such as nuclear obscuration, accretion processes, etc. could be the cause of differing nuclear luminosities within reasonably similar galaxies (with similar black hole masses).

11.2 Morphologies

Recent HST results suggest that luminous nuclear emission predominantly arises from hosts with large spheroidal components (McLure *et al.* 1999). The two least luminous radio-quiet quasars imaged by McLure *et al.* (1999) have disk-like structure at radii $\gtrsim 3$ arcsec, while the more luminous quasars are completely dominated by spheroidal profiles. Could we be seeing a relationship between host morphology and nuclear luminosity? This is particularly interesting when compared to the black hole mass-spheroid mass and spheroid mass-luminosity relations determined for nearby galaxies by Magorrian *et al.* (1998): a large black hole, potentially capable of powering luminous AGN appears more likely to be present in galaxies with large spheroidal components. Both the results of McLure *et al.* (1999) and the relations of Magorrian *et al.* (1998) suggest that quasars with strong nuclear emission should predominantly exist in hosts with large spheroidal components which dominate any disk-like structure.

By careful analysis we have provided evidence that a large fraction of the host galaxies found in this work are dominated by disk-like profiles. However, the most important light for this modelling comes from radii greater than those of the HST study, where the disk component, if present, is expected to be strong. The K -band images described here are not of sufficient quality for us to resolve the inner region and produce a 2-component fit to the host galaxy. This is in contrast to results from HST where the increased resolution enables the inner region to be resolved, and the spheroidal core of the galaxy becomes more important for modelling with a single β parameter. By analysing synthetic data, we have been able to show that for hosts where we find a dominant disk-like component, any additional spheroidal component will not result in a large change in the recovered total host luminosities. We have also provided suggestive evidence that the spheroidal cores of these quasars are of relatively low luminosity. Further analysis of both the regions and profiles probed by different studies, and higher resolution data on the cores of the quasars analysed in this work would be very interesting, and could help

to explain the different morphological results of recent host galaxy studies.

12 CONCLUSIONS

We have presented the results from a deep K -band imaging study designed to reveal the host galaxies of quasars with higher luminosities than targeted by previous studies. Extending host-galaxy studies to these quasars was made possible by the stability provided by the tip-tilt adaptive optics system at UKIRT, which enabled accurate psf measurements to be obtained for the deep quasar images. We have been able to resolve host galaxies for all of our sample.

The principle conclusion of this study is that the luminous quasars in this sample have host galaxies with similar luminosities to quasars of lower total luminosity. Derived nuclear-to-host ratios are therefore larger than those obtained by previous work, and place these quasars beyond the upper limit suggested by studies of quasars with lower total luminosities. Host morphologies are less certain, but there is weak evidence that the hosts of these quasars can be dominated by either disk-like or spheroidal profiles on the scales probed by these images.

13 ACKNOWLEDGEMENTS

The United Kingdom Infrared Telescope is operated by the Joint Astronomy Centre on behalf of the U.K. Particle Physics and Astronomy Research Council.

REFERENCES

Abraham R.G., Crawford C.S., McHardy I.M., 1992, *ApJ*, 401, 474
 Baggett W.E., Baggett S.M., Anderson K.S.J., 1998, *AJ*, 116, 1626
 Bahcall J.N., Kirhakos S., Saxe D.H., Schneider D.P., 1997, *ApJ*, 479, 642
 Bevington P.R., Robinson D.K., 1992, Data reduction and error analysis for the physical sciences, 2nd ed. McGraw-Hill
 Boyce P.J., Disney M.J., Blades J.C., Boksenberg A., Crane P., Deharveng J.M., Macchetto F.D., Mackay C.D., Sparks W.B., 1998, *MNRAS*, 298, 121
 Bruzual A.G., Charlot S., 1993, *ApJ*, 405, 538
 Caon N., Capaccioli M., D'Onofrio M., 1993, *MNRAS* 265, 1013
 Casali M.M., Hawarden T.G., 1992, UKIRT newsletter, 3, 33
 Condon J.J., Cotton W.D., Greisen E.W., Yin Q.F., Perley R.A., Taylor G.B., Broderick J.J., 1998, *AJ*, 115, 1693
 Dunlop J.S., Guiderdoni B., Rocca-Volmerange B., Peacock J.A., Longair M.S., 1989, *MNRAS*, 240, 257
 Dunlop J.S., Taylor G.L., Hughes D.H., Robson E.I., 1993, *MNRAS*, 264, 455
 Efstathiou G., Rees M.J., 1988, *MNRAS*, 230, 5p
 Gardner J.P., Sharples R.M., Frenk C.S., Carrasco B.E., 1997, *ApJ*, 480, L99
 Glazebrook K., Peacock J.A., Miller L., Collins C.A., 1995, *MNRAS*, 275, 169
 Goldschmidt P., Miller L., LaFranca F., Cristiani S., 1992, *MNRAS*, 256, L65
 Haehnelt M.G., Rees M.J., 1993, *MNRAS*, 263, 168
 Hewitt A., Burbidge G., 1993, *AJS*, 87, 451
 Hines D.C., Low F.J., Thompson R.I., Weymann R.J., Storrie-Lombardi L.J., 1999, *ApJ*, 512, 140
 Högbom J.A., 1974, *A&AS*, 15, 417
 Hooper E.J., Impey C.D., Foltz C.B., 1997, *ApJ*, 480, L95
 Hutchings J.B., Crampton D., Campbell B., 1984, *ApJ*, 280, 41
 Hutchings J.B., Neff S.G., 1992, *AJ*, 104, 1
 Hutchings J.B., Neff S.G., Gower A.C., 1992, *PASP*, 104, 62
 Kauffmann G., Haehnelt M., 1999, *MNRAS* submitted, astro-ph/9906493
 Kormendy J., Richstone D., 1995, *ARA&A*, 33, 581
 Lilly S.J., Longair M.S., 1984, *MNRAS*, 211, 833
 Lin H., Kirshner R.P., Schechter P.L., Oemler A., Tucker D.L., Schechter P.L., 1996, *ApJ*, 464, 60
 Magorrian J. *et al.*, 1998, *AJ*, 115, 2285
 Malkan M.A., Margon B., Chanan G.A., 1984a, *ApJ*, 280, 66
 Malkan M.A., 1984b, *ApJ*, 287, 555
 McLeod K.K., Rieke G.H., 1994a, *ApJ*, 420, 58
 McLeod K.K., Rieke G.H., 1994b, *ApJ*, 431, 137
 McLeod K.K., Rieke G.H., 1995, *ApJ*, 441, 96
 McLeod K.K., Rieke G.H., Storrie-Lombardi L.J., 1999, *ApJ*, 511, L67
 McLure R.J., Dunlop J.S., Kukula M.J., Baum S.A., O'Dea C.P., Hughes D.H., 1999, *MNRAS*, 308, 377
 Mobasher B., Sharples R.M., Ellis R.S., 1993, *MNRAS*, 263, 560
 Neugebauer G., Matthews K., Soifer B.T., Elias J.H., 1985, *ApJ*, 298, 275
 Neugebauer G., Green R.F., Matthews K., Schmidt M., Soifer B.T., Bennett J., 1987, *ApJs*, 63, 615
 Pahre M.A., Djorgovski S.G., de Carvalho R.R., 1998, *AJ*, 116, 1591
 Percival W., Miller L., 1999, *MNRAS*, 309, 823
 Percival W., Miller L., 2000, in preparation
 Press W.H., Teukolsky S.A., Vetterling W.T., Flannery B.P., 1992, Numerical recipes in C, 2nd ed. Cambridge Univ. Press
 Smith E.P., Heckman T.M., Bothun G.D., Romanishin W., Balick B., 1986, *ApJ*, 306, 64
 Stockton A., Canalizo G., Close L.M., 1998, *ApJ*, 500, 121
 Taylor G.L., Dunlop J.S., Hughes D.H., Robson E.I., 1996, *MNRAS*, 283, 968
 Veron-Cetty M.P., Woltjer L., 1990, *A&A*, 236, 69